Article

Not peer-reviewed version

Strontium-Doped Mesoporous Bioactive Glass Loading Bisphosphonates Inhibit Osteoclast Differentiation and Prevent Osteoporosis in Ovariectomized Mice

Zhi Zhou , Shicheng Huo * , Zhanchun Li *

Posted Date: 13 November 2023

doi: 10.20944/preprints202311.0754.v1

Keywords: osteoporosis; bioactive glass; strontium; bisphosphonates

Article

Strontium-Doped Mesoporous Bioactive Glass Loading Bisphosphonates Inhibit Osteoclast Differentiation and Prevent Osteoporosis in Ovariectomized Mice

Zhi Zhou [1], Shicheng Huo [2,*] and Zhanchun Li [1,*]

[1] Department of Orthopedics, Renji Hospital, Shanghai Jiaotong University School of Medicine, Shanghai 200127, China. zhouzhi721@163.com

[2] Department of Minimally Invasive Spine, Changzheng Hospital, Chinese People's Liberation Army Navy Military Medical University, Shanghai 200003, China. waznxyz@126.com

* Correspondence: lzctgzyyx@163.com.

Abstract: Postmenopausal osteoporosis, a metabolic bone disease associated with aging and that affects bones throughout the body, is emerging as an urgent public health concern and imposes a substantial healthcare burden on society. The clinical application of bisphosphonate, the primary treatment for osteoporosis, is limited owing to the drug's severe complications. Herein, we investigate the synthesis and utilization of strontium-doped mesoporous bioactive glass loaded with alendronate (ALN@Sr-MBG) as a novel therapeutic agent for osteoporosis, to explore its potential as an alternative to alendronate (ALN). Strontium-doped mesoporous bioactive glass (Sr-MBG) was synthesized using the sol-gel method, while ALN@Sr-MBG was obtained by incorporating Sr-MBG into an alendronate saturated solution. The bioactivities of ALN@Sr-MBG, including biotoxicity, inflammation inhibition, and anti-osteoclast differentiation, were investigated in vitro using CCK-8, flow cytometry, tartrate-resistant acid phosphatase (TRAP) staining, and RT-PCR assays. Animal models were established by surgically removing the ovaries from non-pregnant female C57/BL mice, followed by weekly intraperitoneal injections of ALN@Sr-MBG, ALN, or excipients. After 8 weeks, the mice femurs were extracted and analyzed through Micro-CT scanning, and hematoxylin-eosi, osteoblastic, and osteogenic staining. The *in vitro* findings demonstrated that ALN@Sr-MBG displayed enhanced biological efficacy compared to ALN in terms of inflammation inhibition, osteogenesis promotion, and osteoclastogenesis inhibition. Furthermore, micro-CT analysis revealed that ALN@Sr-MBG significantly augmented bone mineral density (BMD), bone volume fraction (BV/TV), trabecular number (Tb.N), and trabecular thickness (Tb.Th), while reducing trabecular separation (Tb.Sp) and structural model index (SMI) in mice with ovariectomy-induced osteoporosis. The osteoblast and osteogenic staining results indicate the enhanced bioactivities of ALN@Sr-MBG in promoting bone formation and inhibiting bone resorption compared to ALN. *In vitro* and *in vivo* assessments further confirmed that ALN@Sr-MBG exhibits superior anti-osteoporotic bioactivity compared to ALN. The study findings confirm the potential of ALN@Sr-MBG as a novel alternative therapy to ALN and drug candidate for the treatment of osteoporosis.

Keywords: osteoporosis; bioactive glass; strontium; bisphosphonates

1. Introduction

Osteoporosis is a metabolic bone disease that may affect bones throughout the body, and is characterized by decreased bone density, impaired bone strength, and increased susceptibility to fracture. [1] Osteoporosis, a prevalent bone disorder associated with aging, primarily manifests as postmenopausal osteoporosis, making it the most frequently encountered form. Following menopause, a steep reduction in estrogen levels among middle-aged and elderly women disrupts the equilibrium of bone turnover, leading to a substantial imbalance where bone resorption greatly outpaces bone reconstruction and the damage to the bone microstructure triggers osteoporosis.[2] Osteoporotic fractures are a serious yet common consequence of osteoporosis. Approximately half of

 doi:10.20944/preprints202311.0754.v1

the women and a quarter of the men with osteoporosis will suffer at least one fragility fracture during their middle-age and old-age, which can lead to huge healthcare expenditures, ranging from approximately $20 billion in the U.S. to a staggering $130 billion in the European Union. [3] Vertebral and hip fractures are the most common types of fragility fractures, and lead to a decline in physical functioning, severe reduction in quality of life, and increased mortality, and a much higher incidence of recurrent fractures in those who have had an osteoporotic fracture, further exacerbating the treatment dilemma of osteoporosis. [4] As a result, osteoporosis and its complications pose a significant hazard and burden to the health services for all of humanity.

Bisphosphonates, bone resorption inhibitors, are the most widely used anti-osteoporosis drugs. They inhibit osteoclast activity and function to achieve anti-bone resorption. Over the past decades, pharmacologic treatment of osteoporosis has been heavily dependent on bisphosphonate compounds, with more than 30 million prescription orders for alendronate in one year in the United States alone. [5, 6] Bisphosphonates significantly decrease the chances of vertebral and hip fractures, enhance bone density, and increase bone mass in individuals diagnosed with osteoporosis. Moreover, they are deposited in the bone to form a reservoir after prolonged use by the patient and continue to exert anti-fracture efficacy for some time after the patient has stopped taking the drug. [7] However, long-term use of bisphosphonates can lead to rare but serious complications, including osteonecrosis of the jaw and atypical femur fractures.[8-10] For example, the use of alendronate may result in an increased risk of atrial fibrillation or other cardiac arrhythmias. [11] Elderly women may exhibit increased incidence of osteonecrosis of the jaw after receiving intravenous bisphosphonates in the presence of prior history of invasive dental treatment. [12] In addition, atypical femur fractures are also associated with prolonged treatment with bisphosphonates, to the extent that such fractures are referred to as bisphosphonate-associated fractures[9] These dreaded complications have devastated patients' confidence and adherence to undergoing long-term treatment with bisphosphonates.

Bioactive glass (BG) has been used clinically as an alternative material for the treatment of bone disorders for almost 40 years and has been intensively studied based on its use as an osteogenic material.[13] In recent years, BG-containing strontium mesoporous bioactive glass nanoparticles (Sr-MBG) that been found to be promising owing to their high efficacy in treating osteoporosis. [14] The use of strontium for managing osteoporosis has been verified on the clinical drug strontium ranelate. On the one hand, strontium can prolong the survival of osteoblasts and maintain their activity and function; on the other hand, strontium slows down the maturation and differentiation of osteoclasts, reduces the functional activity of osteoclasts, and reduces bone resorption. [15] MBG contains ordered mesopores with a high specific surface area, which can form an apatite surface layer in the solution state and degrade following the rhythm of bone metabolism after attaching to the bone surface. [16, 17] This shows that Sr-MBG is a remarkable drug carrier with anti-osteoporosis activity.

Inspired by the above studies, we investigated whether Sr-MBG-loaded alendronate (ALN), a promising anti-osteoporosis drug, is superior to the sole use of ALN in terms of bone protection. The sequence of events in in vitro experiments demonstrated that the anti-osteoclastic and bone-enhancing effects of ALN@Sr-BGN were superior to those of an equal mass of ALN. Likewise, micro-CT scans and histological analysis of ovariectomized (OVX) mice demonstrated that ALN@Sr-MBG was more active than alendronate alone as a potent preventive agent against osteoporosis. Therefore, our study provides an effective and promising delivery modality for bisphosphonates as a therapeutic approach for postmenopausal osteoporosis.

2. Materials and Methods

2.1. Synthesis of Sr-MBG

We synthesized Sr-MBG using the sol-gel method.[18] Briefly, 3.6 g of CTAB, 200 mg of TEA and 36 ml of ultrapure water were placed in a flask with a volume of 100 ml, magnetically stirred until clarified. Then a mixed solution of TEOS and cyclohexane was slowly added at a certain temperature, and 0.6325 g of calcium nitrate hexahydrate ($Ca(NO_3)_2{\cdot}6H_2O$) was added during stirring for 8 h. While stirring for 1 h, 0.1456 g of strontium nitrate hexahydrate ($Sr(NO_3)_2{\cdot}6H_2O$) was added to 0.051

 doi:10.20944/preprints202311.0754.v1

ml TEP at 9 h of stirring, and the reaction was continued for 12 h to form a sol-gel material. The sol was alternately washed and centrifuged with ethanol and ultrapure water sequentially until the supernatant was clarified, and then hot baked at 60 °C for 72 h to obtain a white solid, which was calcined at a high temperature (600 °C) for 6 h to prepare Sr-MBG.

2.2. Characterization of Sr-MBG

The surface morphology of Sr-MBG was analyzed using a scanning electron microscope (FESEM, ZEISS Gemini SEM 300, Germany). The internal structure and morphological characteristics of Sr-MBG were analyzed using transmission electron microscopy (TEM, FEI Talos F200X G2, USA). The elements of Sr-MBG were characterized by X-ray photoelectron spectroscopy (Thermo Scientific K-Alpha, USA). The crystal structure of Sr-MBG was analyzed using an X-ray diffractometer (Rigaku Ultima IV, Japan). Through analysis, the specific surface area and pore size of Sr-MBG were ascertained via a fully automated rapid specific surface area and void volume analyzer (Micromeritics ASAP 2460, USA) using the BET method. The data obtained were analyzed using Image J, GraphPad Prism 9.0, and origin 8.0.

A suitable quantity of Sr-MBG powder was introduced into the saturated ALN solution, followed by 24 h of agitation in a dark, ambient temperature setting. The mixture was then subjected to centrifugation at 8000 rpm for 10 min, rinsed with deionized water through three cycles of centrifugation, and finally dried at 60°C for 6 h to yield the ALN@Sr-MBG powder. An appropriate amount of ALN@Sr-MBG powder was dissolved in 5 ml of phosphate buffer solution (PBS, pH=7.4) and stirred, and a small amount of the mixed solution of ALN@Sr-MBG and PBS was set aside at different temporal checkpoints (2 h, 4 h, 6 h, 12 h, 24 h, 48 h, 72 h, 96 h, and 120 h) to measure the bisphosphonate accumulation and release concentration of the bisphosphonate in the solution using a method used in previous research. The concentration of bisphosphonate release and make up an equal amount of PBS.[19] Three tests were performed. The data obtained were analyzed and images were plotted using GraphPad Prism 9.0.

2.3. Determination of material toxicity

The mouse-originated macrophage cell line Raw264.7 was seeded in 96-well plates at a concentration of 1×10^4 cells per well and incubated in α-MEM complete medium containing varying quantities of ALN@Sr-MBG. (0, 10, 20, 40, 80, 100, 150, 200, 250 mg/ml) over a span of 1, 3, and 5 days, and utilized the CCK-8 method to determine the cell activity. The data obtained were analyzed using GraphPad Prism 9.0 and images were plotted.

2.4. Cell polarization assay

RAW264.7 cells were seeded into 12-well plates at a concentration of 2×10^4 cells per well, and 50 ng/ml lipopolysaccharide (LPS) was added to each well plate for 2D culture to induce polarization. They were subsequently divided into three groups: the ALN group received 3 μg of alendronate, the ALN@Sr-MBG group received an equivalent dosage of ALN@Sr-MBG, and the control group received an equivalent quantity of the carrier agent. The culture medium was changed every two days and incubated for 5 days.

2.4.1. Flow cytometry

RAW264.7 cells were gently removed from the cell-well plate and washed with PBS twice for 10 min before being placed in 1% fetal bovine serum albumin for 30 min and washed again with PBS. The samples were stained on ice for 1 h in a light-avoiding environment and labeled with isotype coomassie protein (APC)-labeled CD11c and phycoerythrin (PE)-labeled CD206, respectively. Macrophage surface markers M1 (CD11c) and M2 (CD206) were detected by flow cytometry to detect macrophage polarization. The data obtained were analyzed and images were plotted using FlowJo.

2.4.2. Macrophage inflammatory gene expression

 doi:10.20944/preprints202311.0754.v1

The total RNA from each group of cells was extracted using the RNA kit according to the manufacturer's instructions. The cDNA of the samples was synthesized and amplified using the Prime-SCRIPT™RT kit (Takara, Japan) according to the manufacturer's instructions. In the cDNA samples, the expression of genes related to inflammation was assessed following the instructions of the TB Green Premix Ex Taq™Kit kit, with β-actin serving as a control, and data analysis was conducted using the comparative CT method. The resulting data were used to analyze and plot images with GraphPad Prism 9.0.

2.5. In vitro osteoblastic differentiation and assays

Extracted bone marrow macrophages from four-week-old SPF-grade female C57BL/6 mice (Shanghai Jieshijie Laboratory Animal Co., Ltd.) were subjected to in vitro osteoblastic differentiation assay. Summarily, after euthanasia, mouse femoral bone marrow cells were isolated and cultured in α-MEM complete medium containing 10% fetal bovine serum, 1% penicillin/streptomycin, and 50 ng/ml of M-CSF. After 24 h of incubation, the non-adherent cells were removed, and the adherent cells were cultured in an incubator at 37°C and 5% CO_2 until they reached 90% confluence. Mouse bone marrow stromal cells, at a concentration of 1×10^4 cells per well, were introduced into 96-well plates. They were cultured in α-MEM complete medium (comprising 10% fetal bovine serum and 1% dual antibody), with the addition of 30 ng/ml M-CSF and 50 ng/ml RANKL. The cells were randomly assigned to one of three groups, each receiving equivalent volumes of solvent, ALN, or ALN@Sr-MBG. The culture medium was replenished every 48 h, and the incubation was continued for 5 days.

2.5.1. TRAP staining in vitro

After slowly rinsing the osteoclasts in each group with PBS buffer, they were fixed with 4% paraformaldehyde for 15 min and pre-cured with 0.1% Triton X-100 for 5 min. The osteoclasts were subjected to in vitro TRAP staining using the TRAP kit according to the manufacturer's instructions, and we quantified the count of TRAP-positive cells possessing over three nuclei using fluorescence microscopy.

2.5.2. Osteoclast gene expression

We employed qPCR to assess the expression of osteoclast-related genes following the treatment of osteoblasts with ALN and ALN@Sr-MBG. Total RNA was extracted from each group of cells using the RNA kit according to the manufacturer's instructions. cDNA of the samples was synthesized and amplified in accordance with the manufacturer's guidelines for using the Prime-SCRIPT™RT Kit (Takara, Japan). The cDNA samples were used to detect the expression of genes associated with osteoclasts, following the instructions provided with the TB Green Premix Ex Taq™Kit kit. β-actin served as a control, and the data was analyzed using the comparative CT method. The resulting data were used to analyze and plot images using GraphPad Prism 9.0.

2.6. In vitro osteogenic gene expression

We isolated bone marrow mesenchymal stromal cells (BMSC) from female four-week old C57BL/6 mice and met SPF-grade standards (purchased from Shanghai Jieshijie Laboratory Animal Co., Ltd.) for in vitro osteogenic differentiation assay. Summarily, femoral bone marrow cells were harvested after the euthanasia of mice, and then cultured in α-MEM complete medium supplemented with 10% FBS and 1% penicillin/streptomycin. Following a 7-day incubation, non-adherent cells were removed, and adherent cells were cultured in an incubator at 37°C and 5% CO_2 until they reached 90% confluence. The osteogenic induction medium was prepared as described in past research. BMSC were then inoculated in 24-well plates at a density of $2 \times 10_4$ cells per well and cultured using the osteogenic induction medium. The cells were randomly divided into three groups, and equal amounts of solvent, ALN, and ALN@Sr-MBG were added; the culture medium was changed every 2 days for 7 days.

 doi:10.20944/preprints202311.0754.v1

The expression of osteogenesis-related genes after treatment of osteoblasts with ALN and ALN@Sr-MBG was detected using qPCR. Total RNA was extracted from each group of cells according to the RNA kit instructions. The cDNA of the samples was synthesized and amplified using the Prime-SCRIPT™RT Kit (Takara, Japan) in accordance with the manufacturer's instructions. The cDNA samples were used to analyze the expression of genes associated with osteogenesis, following the provided instructions for the TB Green Premix Ex Taq™Kit kit; β-actin served as a control, and data analysis was performed utilizing the comparative CT method. The resulting data were used to analyze and plot images with GraphPad Prism 9.0.

2.7. Animal experiments

Twenty-four female C57BL/6 mice, 12 weeks old and adherent to SPF-grade standards (purchased from Shanghai Jieshijie Laboratory Animal Co., Ltd.), were acclimatized for 1 week and then randomly divided into 4 groups: sham-operated group (SHAM + excipient injections), OVX group (OVX + excipient injections), bisphosphonate group (OVX + 5 mg/kg ALN injections), and strontium-doped bioactive vitrona-loaded bisphosphonate group (OVX + 5 mg/kg ALN@Sr-MBG injection). All animal surgeries performed in this study were in accordance with the National Institutes of Health Guide for the Care and Use of Laboratory Animals and were approved by the Animal Ethics Committee of Renji Hospital, Shanghai Jiao Tong University (Shanghai, China) (Animal Ethics Committee Approval No. RJ2018-1012). Under aseptic conditions, mice underwent bilateral ovariectomy or sham surgery under general anesthesia, and the wounds were carefully sutured after surgery. Following a week of recovery, the mice were subjected to intraperitoneal injections once a week for eight weeks, and their weights were recorded weekly.

All mice were euthanized at the end of the experiment and their femurs were removed for micro-CT analysis and histological observation. The microstructural changes of mouse femurs were observed using a high-resolution micro-CT scanner (SkyScan-1176, Belgium) and bone parameters such as bone mineral density (BMD), bone trabecular bone volume fraction (BV/TV), structural model index (SMI), trabecular spacing (Tb.Sp), trabecular number (Tb.N), and trabecular thickness (Tb.Th) were analyzed by scanning software.

Mouse femurs were decalcified in 10% EDTA for approximately 4 weeks, then paraffin-embedded, and the specimens were subjected to hematoxylin-eosin (HE), TRAP, and osteogenic staining.

2.8. Statistics

The data are presented as mean ± SD (standard deviation of the mean) and analyzed using GraphPad Prism 9.0 (GraphPad Software Inc, CA, USA) with group comparisons conducted through one-way ANOVA, indicating statistical significance at p-value < 0.05.

3. Results

3.1. Characterization of Sr-MBG

The various characterizations of Sr-MBG are shown in Figure 1. The scanning electron microscopy and transmission electron microscopy results (Figure 1 a, b) show that Sr-MBG has a spherical structural morphology and mesoporous structure with good dispersion and homogeneity. From the particle size distribution graph (Figure 1 c), the particle size of Sr-MBG is basically distributed within the range of 100-125 nm, and the average particle size is about 113.60 nm. The composition of Sr-MBG was qualitatively analyzed using XPS, and the results (Figure 1 d, e, f, g, h, i) indicate that Sr-MBG consists mainly of the elements Si and O, in addition to small amounts of Ca and trace amounts of Sr owing to its low peak value.

Preprints (www.preprints.org) | NOT PEER-REVIEWED | Posted: 13 November 2023 doi:10.20944/preprints202311.0754.v1

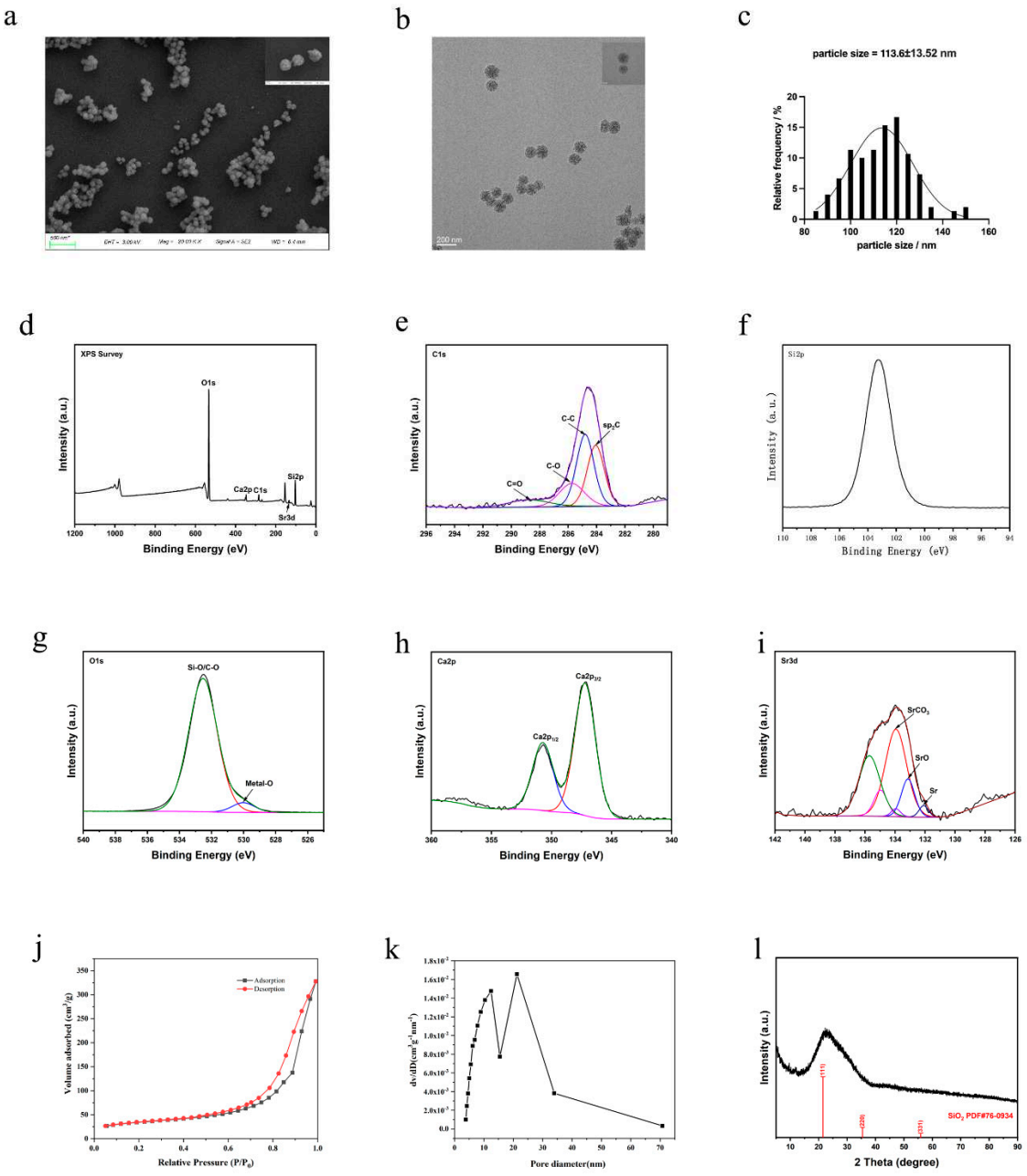

Figure 1. Material characterization of Sr-MBG. a is the scanning electron microscopy of Sr-MBG; b is the transmission electron microscopy of Sr-MBG; c represents the size distribution of Sr-MBG particles; d, e, f, g, h, and i represent the XPS analysis of Sr-MBG; j is the nitrogen adsorption-desorption isotherm of Sr-MBG; k is the pore size distribution of Sr-MBG; and l is the XRD analysis of Sr-MBG.

The nitrogen adsorption-desorption isotherms of Sr-MBG obtained by BET analysis (Figure 1 j) belonged to type IV isotherms and had H3 hysteresis lines, indicating that Sr-MBG had a mesoporous structure, agreeing with the results of electron microscopy observations. Figure 1k shows that most of the Sr-MBG mesopore pore sizes range between 12 and 22 nm. Figure 1l shows the XRD diffractogram of Sr-MBG. Figure 1l illustrates the amorphous nature of Sr-MBG (broad peaks at 2θ = 20°-32°). In summary, Sr-MBG has good specific surface area and amorphous structure, which provides a good material structure basis for loading bisphosphonates.

3.2. Biotoxicity and drug release of ALN@Sr-MBG

Preprints (www.preprints.org) | NOT PEER-REVIEWED | Posted: 13 November 2023 doi:10.20944/preprints202311.0754.v1

The RAW264.7 cell line, a mouse monocyte macrophage-derived tumor cell, was selected for testing ALN@Sr-MBG biotoxicity owing to its homology to macrophages capable of differentiating into osteoclasts and its easy accessibility.

The results of CCK8 (Figure 2 a, b, c) show that ALN@Sr-MBG within the concentration of 0-100 mg/ml is not cytotoxic, and ALN@Sr-MBG within the concentration of 100-200 mg/ml does not suggest cytotoxicity until the fifth day. Therefore, as far as material toxicity is concerned, ALN@Sr-MBG within the concentration of 0-100 mg/ml is safe for cells. As seen in Figure 2 d, there was a burst release of ALN@Sr-MBG in the first 12 h; by the 5th day afterwards, ALN@Sr-MBG was still continuously and gradually releasing alendronate. This indicates that ALN@Sr-MBG has a good slow-release effect.

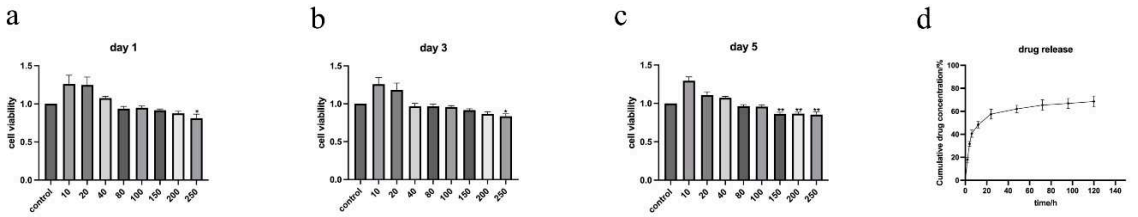

Figure 2. Biotoxicity and drug release of ALN@Sr-MBG. a, b, and c are the CCK8 results of different concentrations of ALN@Sr-MBG-treated cells on days 1, 3, and 5. * denotes that the p-value for this group is <0.05 compared to the control group, ** indicates a p-value <0.01 compared to the control group. d is the concentration profiles of the drug released from ALN@Sr-MBG over time.

3.3. Effect of ALN@Sr-MBG on inflammatory cell polarization in vitro

Detection of the effect of ALN@Sr-MBG on inflammatory cell polarization was accomplished by flow cytometry and RT-PCR. In the flow cytometry results, the Q1 region is the percentage of CD11c-positive cells, namely M1-type macrophages, and the Q4 region is the percentage of CD206-positive cells, namely M2-type macrophages. As shown in Figure 2. a, b, and c, both ALN and ALN@Sr-MBG reduced the proportion of M1-type macrophages, indicating that both ALN and ALN@Sr-MBG reversed inflammatory cell polarization.

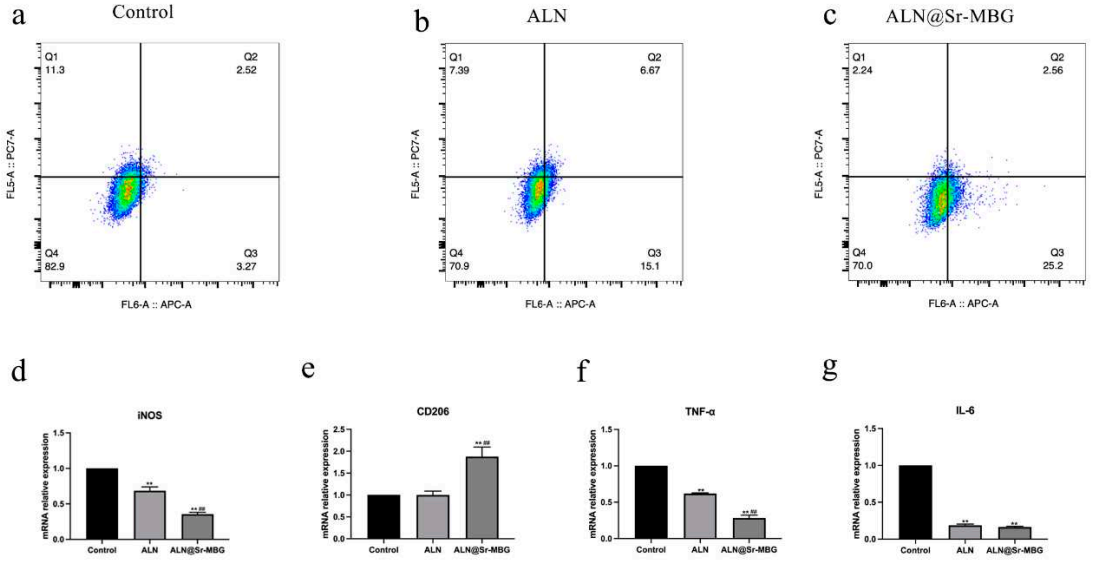

Figure 3. Effect of ALN@Sr-MBG on polarization of inflammatory cells. a, b, and c are the cell flow results of the cells in each group; d, e, f, and g are the expression of inflammation-related genes in the cells in each group. ** signifies that the group exhibits a p-value <0.01 compared to the Control group, and ## indicates a p-value <0.01 relative to the ALN group.

Furthermore, there was a decreased proportion of CD206-positive cells (M2-type macrophages) in the ALN@Sr-MBG group compared to the Control and ALN groups, indicating a higher tendency

Preprints (www.preprints.org) | NOT PEER-REVIEWED | Posted: 13 November 2023 doi:10.20944/preprints202311.0754.v1

of ALN@Sr-MBG-treated macrophages to differentiate into M2-type macrophages. Additionally, as shown by the RT-PCR results, both ALN and ALN@Sr-MBG downregulated inflammatory genes associated with M1 polarization, such as iNOS, TNF-α, and IL-6, but only ALN@Sr-MBG upregulated genes associated with M2-type macrophages, namely CD206. Therefore, both ALN and ALN@Sr-MBG inhibited macrophage polarization toward M1, but only ALN@Sr-MBG promoted macrophage differentiation toward M2.

3.4. Effect of ALN@Sr-MBG on osteoclast differentiation in vitro

The morphology of mature osteoclasts is multinucleated giant cell morphology. Therefore, this characteristic of osteoclasts can be utilized to verify whether ALN and ALN@Sr-MBG can effectively inhibit RANKL-induced osteoclast generation and differentiation. Figure 3 shows the differentiation of osteoclasts in each group. Whether the macrophages in each group were maturely differentiated into osteoclasts was determined through TRAP staining, and the results are demonstrated in Figure 4 a, b, and c. Figure 4 d shows the number of mature osteoclasts in each group.

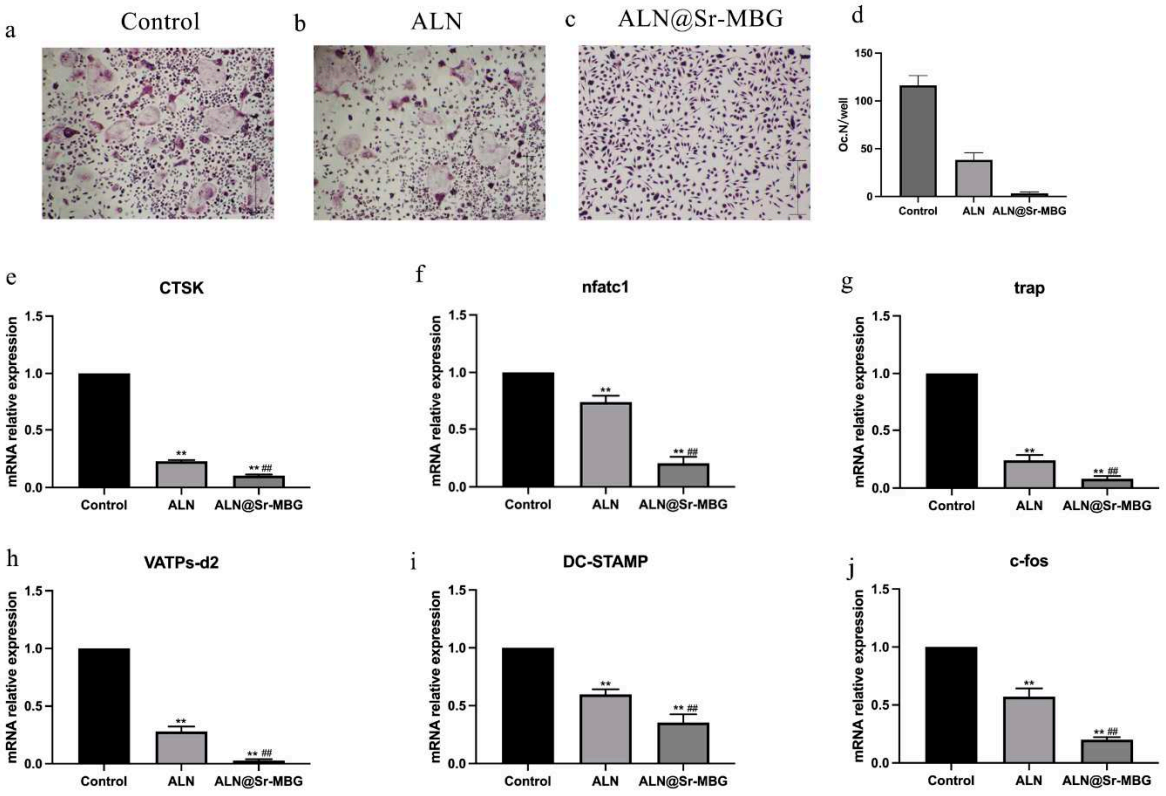

Figure 4. Effect of ALN@Sr-MBG on osteoclast differentiation in vitro. a, b, and c are the results of TRAP staining of osteoblasts in each group; d is the number of osteoblasts in each group; e, f, g, h, i and j are the expressions of osteoblast-related genes in each group; ** indicates that the group has a p-value of <0.01 compared with the control group, and ## indicates that the group has a p-value of <0.01 compared with the ALN group.

TRAP staining results demonstrated a significant hindrance in osteoclast differentiation in both the ALN and ALN@Sr-MBG groups compared to the control group. In Figure 4d, the ALN group and ALN@Sr-MBG group exhibited a notably reduced osteoclast count compared to the control group. Moreover, ALN@Sr-MBG had a stronger inhibitory effect on osteoclast differentiation compared to the ALN group. In the presence of ALN@Sr-MBG, bone marrow macrophages could hardly differentiate into osteoclasts. Figure 4 illustrates that ALN@Sr-MBG has potent anti-osteoclast differentiation activity in vitro.

3.5. ALN@Sr-MBG ameliorates bone loss in OVX mice in vivo to delay osteoporosis

Preprints (www.preprints.org) | NOT PEER-REVIEWED | Posted: 13 November 2023 doi:10.20944/preprints202311.0754.v1

Postmenopausal osteoporotic individuals suffer from estrogen deficiency owing to loss of ovarian function. Therefore, we produced a mouse model of osteoporosis by surgically removing the ovaries of female mice to establish an estrogen-deficient environment, which was used to verify the effect of ALN@Sr-MBG on osteoporosis *in vivo*. The bone mass of mice in each group is shown by Figure 5a. Figure 5b displays the outcomes for diverse mouse bone parameters. Compared to the OVX group, both the ALN and ALN@Sr-MBG groups exhibited a substantial increase in bone mass, indicating their effectiveness in ameliorating bone loss in osteoporotic individuals. Simultaneously, ALN@Sr-MBG demonstrated a notable increase in bone mass compared to the ALN group, indicating a more potent reversal of osteoporotic bone loss with ALN@Sr-MBG than with ALN. This is also illustrated by the changes in bone parameters in each group. Therefore, as shown in Figure 5, ALN@Sr-MBG exhibits potent anti-osteoporotic activity in vivo.

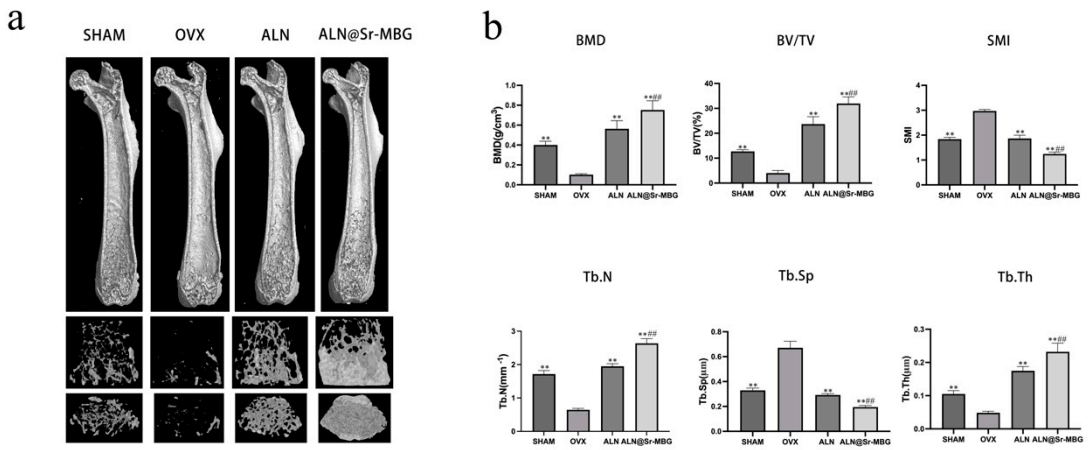

Figure 5. Effect of ALN@Sr-MBG on bone mass in OVX mice. a shows the results of femur Micro-CT in each group of mice; b shows the results of each bone parameter in each group of mice, ** signifies a p-value <0.01 compared to the OVX group, and ## indicates a p-value <0.01 relative to the ALN group.

3.6. Anti-osteoclastic activity of ALN@Sr-MBG in vivo

The *in vivo* anti-osteoclast activity of ALN@Sr-MBG was verified by HE and TRAP staining of sections of isolated mouse femurs after decalcification and embedding, the results of which are shown in Figure 6.

Preprints (www.preprints.org) | NOT PEER-REVIEWED | Posted: 13 November 2023 doi:10.20944/preprints202311.0754.v1

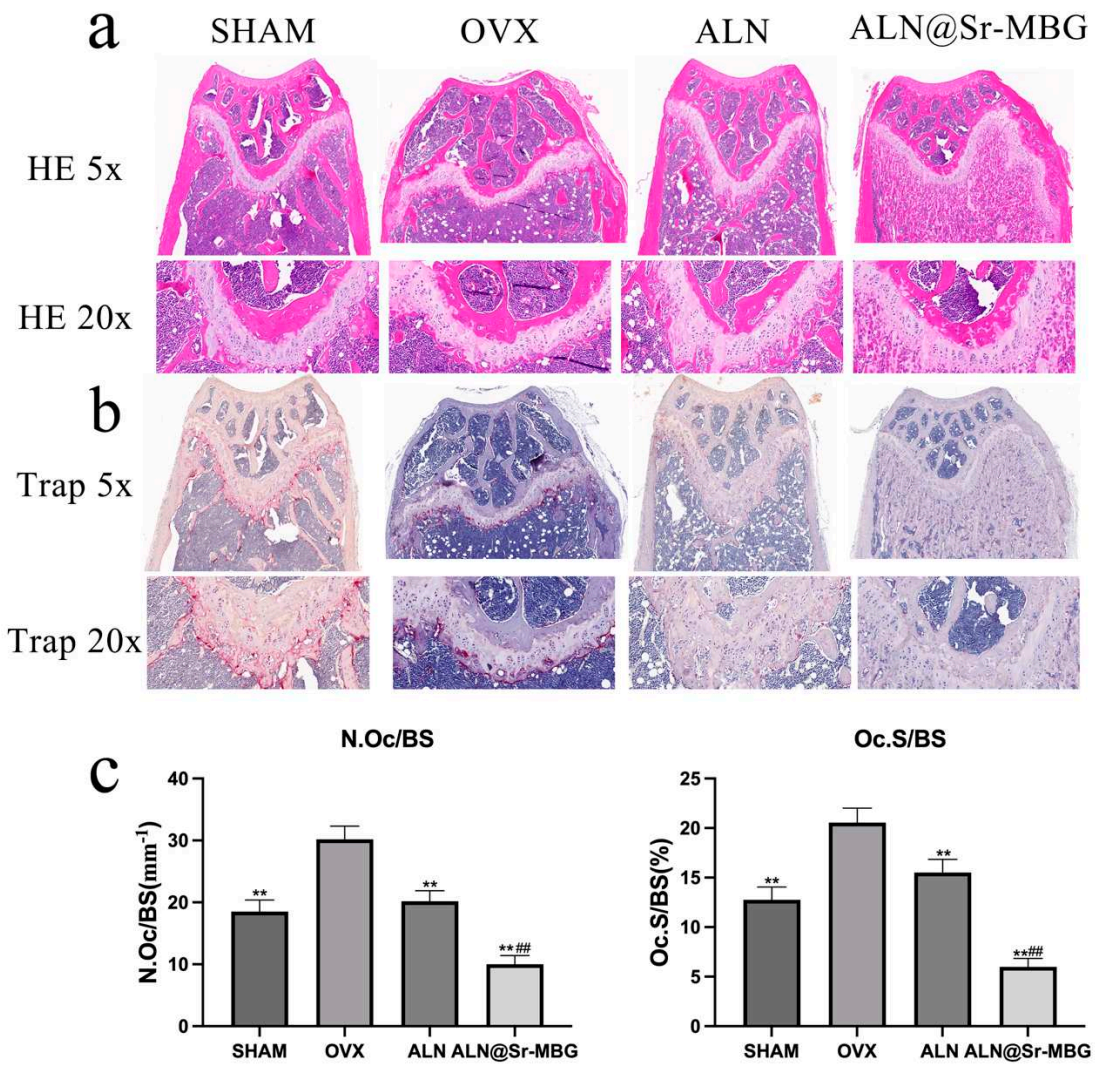

Figure 6. Anti-osteoclast activity of ALN@Sr-MBG *in vivo*. a displays the outcomes of HE staining for the femur of mice in each group; b illustrates the results of TRAP staining for the femur of mice in each group; and c showcases the quantity and area of osteoclasts in TRAP staining for the femur of mice in each group; ** denotes a comparison with the OVX group, yielding a p-value <0.01, and ## signifies a comparison with the ALN group, also resulting in a p-value <0.01.

Figure 6 a displays the outcomes of femur HE staining in each group of mice, Figure 6 b illustrates the results of femur TRAP staining in each group, and Figure 6 c depicts the count and area of osteoclasts in femur TRAP staining among the groups of mice. Both SHAM and OVX groups showed strong positive TRAP staining results, and the TRAP staining activity in both the ALN and ALN@Sr-MBG groups exhibited notable suppression compared to the OVX group, signifying the robust in vivo anti-osteoclastogenic effects of both ALN and ALN@Sr-MBG. As shown in Figure 6 c, the number and relative area ratio of TRAP-positive osteoclasts in both the ALN and ALN@Sr-MBG groups were smaller than that in the OVX group, and at the same time, the inhibitory effect on osteoclast activity was stronger in the ALN@Sr-MBG than in the ALN. Therefore, as shown in Figure 6, ALN@Sr-MBG exhibits potent in vivo anti-osteoclast activity.

3.7. ALN@Sr-MBG promotes osteogenic activity in vitro and in vivo

After decalcifying, embedding, and sectioning the isolated femur of each group of mice, the sections were stained for osteogenic staining, and the staining results are shown in Figure 7 a and b. Primary mouse BMSC cells were extracted for *in vitro* culture and osteogenic differentiation. The RNA of osteoblasts cultured in each group was extracted for RT-PCR to detect the expression of

Preprints (www.preprints.org) | NOT PEER-REVIEWED | Posted: 13 November 2023 doi:10.20944/preprints202311.0754.v1

osteogenesis-related genes, and the results are shown in Figure 7 c. As shown by the osteogenic staining of mouse femur, the number and area of osteoblasts in the ALN and ALN@Sr-MBG group were significantly larger than those in the OVX group, suggesting that both have osteogenesis-promoting effects in vivo. Compared to the ALN group, the ALN@Sr-MBG group displayed a significant increase in osteoblast count. Furthermore, the in vitro disparity in osteogenic gene expression between the ALN and ALN@Sr-MBG groups corresponded with the in vivo findings, indicating a stronger osteogenic promoting effect of ALN@Sr-MBG compared to ALN. Figure 7 illustrates that ALN@Sr-MBG has a strong osteogenesis-promoting effect *in vitro* and *in vivo*.

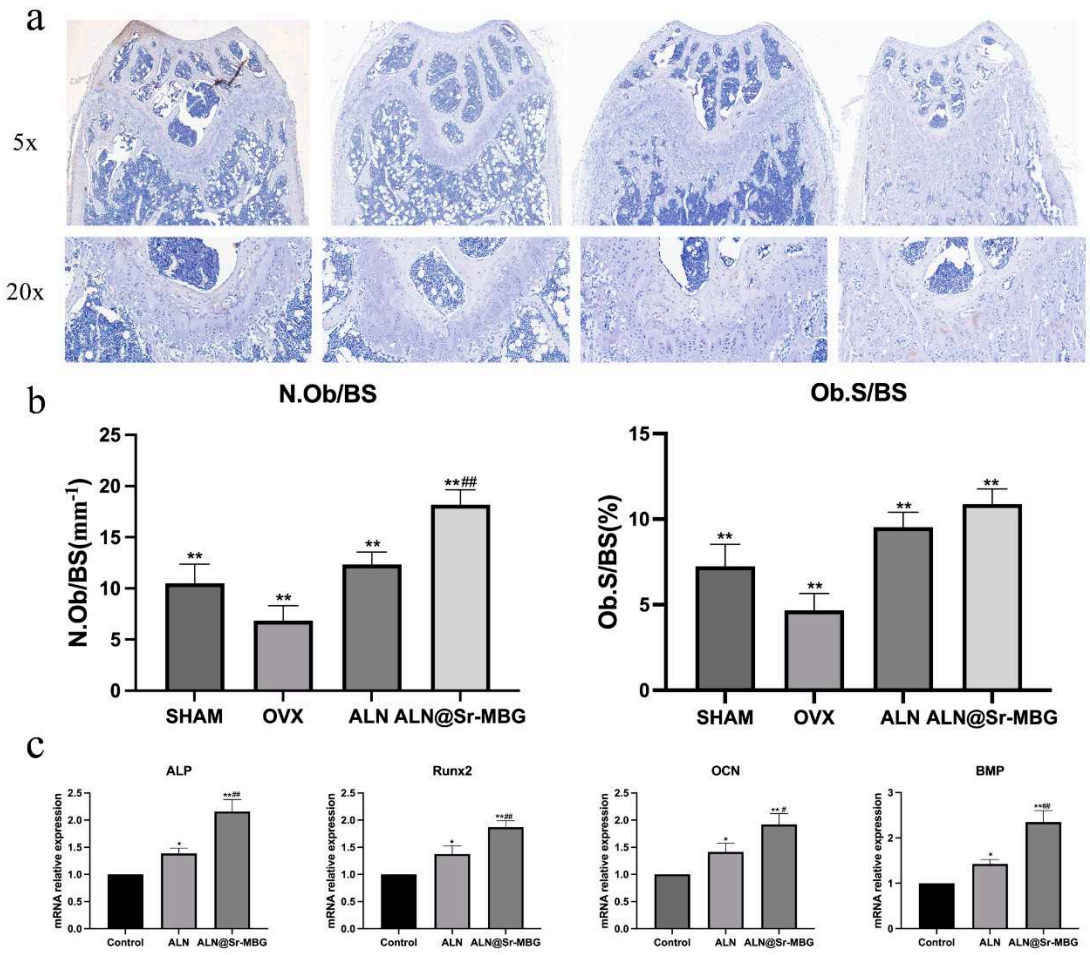

Figure 7. ALN@Sr-MBG promotes osteogenic activity *in vitro* and *in vivo*. a is the result of osteogenic staining of mouse femurs in each group; b is the number and area of osteoblasts in osteogenic staining of mouse femur in each group, ** indicates the p-value of this group compared with that of the OVX group <0.01, ## indicates the p-value of this group compared with that of the ALN group <0.01. c is the expression of osteogenic genes in osteoblasts for each group *in vitro*, * signifies a p-value <0.05 compared with the control group, ** denotes a p-value <0.01 compared to the control group, # indicates a p-value <0.05 relative to the ALN group, and ## indicates a p-value <0.01 relative to the ALN group.

4. Discussion

A dynamic balance is observed between bone resorption and bone formation in normal bone tissue, a process known as bone remodeling, which is an important means of maintaining bone renewal. In osteoporotic individuals, the activation of osteoclasts or inactivation of osteoblasts owing to various reasons leads to an uncoupling of bone resorption and bone formation, disturbances in bone remodeling, and deterioration of the bone microarchitecture, which are macroscopically manifested by reductions in the amount of bone and bone quality, and the susceptibility to fragility fracture. Estrogen deficiency is a predominant and significant contributor to bone metabolism

 doi:10.20944/preprints202311.0754.v1

imbalances, making postmenopausal osteoporosis the most prevalent form of osteoporosis.[20] Fragility fracture is the most serious complication of osteoporosis; it seriously jeopardizes the quality of life and longevity of the osteoporotic population, and imposes a huge economic burden on society.

The treatment of osteoporosis is very diverse, with estrogen replacement therapy, antiresorptive bisphosphonates, and RANKL inhibitors, among which bisphosphonates are used as first-line of anti-osteoporosis drugs owing to their advantages of being inexpensive, easy to obtain, and relatively safe.[21] However, prolonged bisphosphonate usage leads to concerning complications, such as osteonecrosis of the jaw and atypical femur fractures, which are often associated with the frequency and dose of bisphosphonate use. Therefore, new alternative therapies are needed to reduce the dose and frequency of bisphosphonates and thus circumvent these risks.

Strontium is extensively used in anti-osteoporosis research as an important component of anti-osteoporosis biomaterials. Strontium ranelate began to play an important role as an anti-osteoporosis drug as early as the beginning of the 21st century.[22] Wang et al. applied a strontium-containing coating to an intramedullary nail made of magnesium alloy and implanted it in the femur of rats, and found that strontium promoted fracture healing by increasing osteogenic activity.[23] By synthesizing strontium-substituted bioactive glasses, Liu et al. found that strontium has both bone-enhancing and antimicrobial effects in vitro.[24] By synthesizing Sr-SBG, Zhang et al. found that it could promote the proliferation and differentiation of BMSC cells toward osteoblasts, and these functions might be related to the significant up-regulation of β-catenin/Wnt signaling pathway-related proteins by Sr-SBG.[25]

In this study, we designed and synthesized the system ALN@Sr-MBG and demonstrated in vitro and in vivo that ALN@Sr-MBG has stronger anti-osteoporotic bioactivity than ALN alone. CCK8 experiments confirmed the safety of ALN@Sr-MBG, demonstrating that ALN@Sr-MBG is not cytotoxic within the concentration range for inhibiting osteoclast differentiation. The TRAP assay showed that both ALN and ALN@Sr-MBG significantly reduced the number of mature osteoclasts. While the inhibitory effect of ALN@Sr-MBG was significantly stronger than that of ALN in the presence of ALN@Sr-MBG, the BMM could hardly differentiate into osteoclasts. Flow cytometry indicated that although both ALN and ALN@Sr-MBG reversed the M1-type polarization of macrophages, only ALN@Sr-MBG promoted the polarization of macrophages in the M2 direction, suggesting that the inhibitory effect on inflammation of ALN@Sr-MBG was stronger than that of ALN in vitro. The RT-PCR findings indicated that ALN@Sr-MBG notably suppressed the expression of inflammatory and osteoblastic genes while significantly enhancing the expression of osteogenic genes. These findings suggest that at equivalent doses, ALN@Sr-MBG significantly inhibits inflammation and osteoclast differentiation and promotes osteogenic gene expression in vitro compared to ALN, and may be a potential option for anti-osteoporosis.

To verify the anti-osteoporotic effect of ALN@Sr-MBG in vivo, we used OVX mice as animal models of osteoporosis for the relevant experiments. Consistent with the in vitro results, ALN@Sr-MBG ameliorated estrogen deficiency-induced osteoporotic bone loss, significantly increased the number and thickness of trabeculae, shortened the trabecular spacing, and improved BV/TV and BMD in the treatment group. In addition, osteoclastic and osteoblastic staining reflected the potent anti-bone resorption and pro-bone formation bioactivities of ALN@Sr-MBG in vivo. Therefore, our in vivo experiments demonstrated the effective anti-osteoporotic activity of ALN@Sr-MBG. At the same time, we found that ALN alone required relatively high dose and frequency to achieve therapeutic effects at par with ALN@Sr-MBG. Therefore, the use of ALN@Sr-MBG as an alternative therapy to ALN can significantly reduce the dose and frequency of ALN, thus effectively circumventing the risk of complications associated with long-term bisphosphonate use.

We have demonstrated that ALN@Sr-MBG, as an alternative therapy to ALN, is a potential option for the treatment of osteoporosis. However, the mechanism underlying the anti-osteoporosis activity of ALN@Sr-MBG has not been elucidated, and a Sr-MBG-related drug is lacking in the market; therefore, the safety and clinical utility of ALN@Sr-MBG need to be further investigated. Further exploration is also needed for the dosage form of ALN@Sr-MBG, the dosage to be used, and

the mode of administration. Therefore, ALN@Sr-MBG requires further development to become a viable pharmaceutical option for osteoporosis.

Summarily, our findings indicate that ALN@Sr-MBG effectively suppresses bone resorption and enhances bone formation both in vivo and in vitro, thereby mitigating osteoporosis-induced bone loss and reducing the risk of fracture. Moreover, ALN@Sr-MBG can significantly reduce the dosage and frequency of ALN use thereby avoiding the associated drug risks and improving its safety, making it an effective alternative therapy and drug candidate for bisphosphonate treatment of osteoporosis. However, further research of ALN@Sr-MBG as a clinical drug in the context of future drug development is needed; however, the drug is a potent and potent potential anti-osteoporotic agent.

Author Contributions: Zhi Zhou, conceptualization, methodology, investigation, writing—original draft preparation, data curation; Shicheng Huo, conceptualization, formal analysis, methodology, investigation, data curation, visualization, project administration; Zhanchun Li, writing—review and editing, supervision, resources, funding acquisition, project administration. All authors have read and agreed to the published version of the manuscript.

Funding: This research was funded by Shanghai Municipal Science and Technology Commission Program Project, (No. 21140904600) and Shanghai Municipal Health Commission Program Project, (No. 202340081).

Data Availability Statement: Data are contained within the article.

Acknowledgments:

Conflicts of Interest: The authors declare no conflict of interest.

References

1. Aibar-Almazán, A.; Voltes-Martínez, A.; Castellote-Caballero, Y.; Afanador-Restrepo, D.F.; Carcelén-Fraile, M.D.C.; López-Ruiz, E. Current status of the diagnosis and management of osteoporosis. *Int J Mol Sci* **2022**, 23(16).
2. Arceo-Mendoza, R.M.; Camacho, P.M. Postmenopausal osteoporosis: Latest guidelines. *Endocrinol Metab Clin North Am* **2021**, *50(2)*, 167–78.
3. Zhang, S.; Huo, S.; Li, H.; Tang, H.; Qu, X.; Yue, B. Flufenamic acid inhibits osteoclast formation and bone resorption and act against estrogen-dependent bone loss in mice. *Int Immunopharmacol* **2020**, *78*, 106014.
4. Lane, N.E. Epidemiology, etiology, and diagnosis of osteoporosis. *Am J Obstet Gynecol* **2006**, *194(2 Suppl)*, S3–11.
5. Cummings, S.R.; Santora, A.C.; Black, D.M.; Russell, R.G.G. History of alendronate. *Bone* **2020**, *137*, 115411.
6. Tella, S.H.; Gallagher, J.C. Prevention and treatment of postmenopausal osteoporosis. *J Steroid Biochem Mol Biol*, **2014**, *142*, 155–70.
7. Cremers, S.; Drake, M.T.; Ebetino, F.H.; Bilezikian, J.P.; Russell, R.G.G. Pharmacology of bisphosphonates. *Br J Clin Pharmacol*, **2019**, *85(6)*, 1052–62.
8. Krueger, C.D.; West, P.M.; Sargent, M.; Lodolce, A.E.; Pickard, A.S. Bisphosphonate-induced osteonecrosis of the jaw. *Ann Pharmacother*, **2007**, *41(2)*, 276–84.
9. Yano, Y.; Kuriyama, A.; Yano, Y.; Takeshita, A.; Hashizume, H. Atypical femoral fracture with bisphosphonate use. *QJM Int J Med* **2020**, *113(11)*, 825–6.
10. Adami, G.; Jaleel, A.; Curtis, J.R.; Delzell, E.; Chen, R.; Yun, H.; Daigle, S.; Arora, T.; Danila, M.I.; Wright, N.C.; Cadarette, S.M. Temporal trends and factors associated with bisphosphonate discontinuation and restart. *J Bone Miner Res* **2020**, *35(3)*, 478–87.
11. Pazianas, M.; Compston, J.; Huang, C.L.H. Atrial fibrillation and bisphosphonate therapy. *J Bone Miner Res*, **2010**, *25(1)*, 2-10.
12. Ruggiero, S.L.; Mehrotra, B. Bisphosphonate-related osteonecrosis of the jaw: diagnosis, prevention, and management. *Annu Rev Med* **2009**, *60*, 85–96.
13. Fernandes, J.S.; Gentile, P.; Pires, R.A.; Reis, R.L.; Hatton, P.V. Multifunctional bioactive glass and glass-ceramic biomaterials with antibacterial properties for repair and regeneration of bone tissue. *Acta Biomater* **2017**, *59*, 2–11.
14. Zhang, J.; Zhao, S.; Zhu, Y.; Huang, Y.; Zhu, M.; Tao, C.; Zhang, C. Three-dimensional printing of strontium-containing mesoporous bioactive glass scaffolds for bone regeneration. *Acta Biomater* **2014**, *10(5)*, 2269–81.
15. Kołodziejska, B.; Stępień, N.; Kolmas, J. The influence of strontium on bone tissue metabolism and its application in osteoporosis treatment. *Int J Mol Sci* **2021**, *22(12)*.

16. Schumacher, M.; Habibovic, P.; Van Rijt, S. Mesoporous bioactive glass composition effects on degradation and bioactivity. *Bioact Mater*, **2021**, *6(7)*, 1921–31.
17. Workie, A.B.; Sefene, E.M. Ion-doped mesoporous bioactive glass: preparation, characterization, and applications using the spray pyrolysis method. *RSC Adv*, **2022**, *12(3)*, 1592–603.
18. Huo, S.; Wang, F.; Lyu, Z.; Hong, Q.; Wei, J.; Wang, Y.; Zhang, J.; Yue, B. Dual-functional polyetheretherketone surface modification for regulating immunity and bone metabolism. *Chem Eng J* **2021**, *426*, 130806.
19. Bose, S.; Vu, A.A.; Emshadi, K.; Bandyopadhyay, A. Effects of polycaprolactone on alendronate drug release from Mg-doped hydroxyapatite coating on titanium. *Mater Sci Eng C Mater Biol Appl*, **2018**, *88*, 166–71.
20. Li, J.; Chen, X.; Lu, L.; Yu, X. The relationship between bone marrow adipose tissue and bone metabolism in postmenopausal osteoporosis. *Cytokine Growth Factor Rev* **2020**, *52*, 88–98.
21. Brown, J.P. Long-term treatment of postmenopausal osteoporosis [J]. *Endocrinol Metab (Seoul)* **2021**, *36(3)*, 544–52.
22. O'Donnell, S.; Cranney, A.; Wells, G.A.; Adachi, J.; Reginster, J.Y. Strontium ranelate for preventing and treating postmenopausal osteoporosis. *Cochrane Database Syst Rev* **2006**, *2006(4)*, Cd005326.
23. Wang, Z.; Wang, X.; Pei, J.; Tian, Y.; Zhang, J.; Jiang, C.; Huang, J.; Pang, Z.; Cao, Y.; Wang, X.; An, S. Degradation and osteogenic induction of a SrHPO(4)-coated Mg-Nd-Zn-Zr alloy intramedullary nail in a rat femoral shaft fracture model. Biomaterials, **2020**, *247*, 119962.
24. Liu, J.; Rawlinson, S.C.; Hill, R.G.; Fortune, F. Strontium-substituted bioactive glasses in vitro osteogenic and antibacterial effects. *Dent Mater*, **2016**, *32(3)*, 412–22.
25. Zhang, W.; Huang, D.; Zhao, F.; Gao, W.; Sun, L.; Li, X.; Chen, X. Synergistic effect of strontium and silicon in strontium-substituted sub-micron bioactive glass for enhanced osteogenesis. *Mater Sci Eng C Mater Biol Appl* **2018**, *89*, 245–55.